Dermal Patch with Integrated Flexible Heater for on Demand Drug Delivery

*Sara Bagherifard, Ali Tamayol, Pooria Mostafalu, Mohsen Akbari, Mattia Comotto, Nasim Annabi, Masoumeh Ghaderi, Sameer Sonkusale, Mehmet R. Dokmeci, and Ali Khademhosseini**

Topical administration of drugs and growth factors in a controlled fashion can improve the healing process during skin disorders and chronic wounds. To achieve this goal, a dermal patch is engineered that utilizes thermoresponsive drug microcarriers encapsulated within a hydrogel layer attached to a flexible heater with integrated electronic heater control circuitry. The engineered patch conformally covers the wound area and enables controlled drug delivery by electronically adjusting the temperature of the hydrogel layer. The drugs are encapsulated inside microparticles in order to control their release rates. These monodisperse thermoresponsive microparticles containing active molecules are fabricated using a microfluidic device. The system is used to release two different active molecules with molecular weights similar to drugs and growth factors and their release profiles are characterized. This platform is a key step towards engineering smart and closed loop systems for topical applications.

1. Introduction

Skin is the largest organ in the body. It helps regulating body temperature and forms a barrier creating a closed environment to protect the internal tissues from pathogens and variations in environmental conditions.[1] Skin possesses self-renewal characteristics, which help with the repair and regeneration of injuries and cuts. However, in some cases such as burns, deep cuts, diabetes, and infections, the self-healing capability of skin is impaired and further intervention such as growth factor delivery is required.[2] In many of these disorders, the microvessels are damaged and the blood supply to the injured tissue is limited. Therefore, high doses of systemically administered drugs are required to achieve sufficient therapeutic effects. Such high doses may lead to adverse drug reactions including toxicity or other side effects associated with the pharmacokinetic properties of the drug.[3] Sustained localized drug delivery is a promising technique to prevent these side effects. In addition, due to the large exposed surface area of the skin, epidermal drug delivery is an attractive approach for administering the drugs that are not easy to absorb orally or nasally.[4] Thus, the development of epidermal

Dr. S. Bagherifard, Dr. A. Tamayol, Prof. M. Akbari, M. Comotto, Prof. N. Annabi, Dr. M. Ghaderi, Dr. M. R. Dokmeci, Prof. A. Khademhosseini
Biomaterials Innovation Research Center
Department of Medicine
Brigham and Women's Hospital
Harvard Medical School
Cambridge, MA 02139, USA
E-mail: alik@rics.bwh.harvard.edu

Dr. S. Bagherifard, Dr. A. Tamayol, Prof. M. Akbari, M. Comotto, Prof. N. Annabi, Dr. M. Ghaderi, Dr. M. R. Dokmeci, Prof. A. Khademhosseini
Harvard-MIT Division of Health Sciences and Technology
Massachusetts Institute of Technology
Cambridge, MA 02139, USA

Dr. S. Bagherifard
David H. Koch Institute for Integrative Cancer Research
Massachusetts Institute of Technology
Cambridge, MA 02139, USA

Dr. S. Bagherifard
Department of Mechanical Engineering
Politecnico di Milano
Milan 20156, Italy

Dr. A. Tamayol, Prof. M. Akbari, Prof. N. Annabi, Dr. M. R. Dokmeci, Prof. A. Khademhosseini
Wyss Institute for Biologically Inspired Engineering
Harvard University
Boston, MA 02115, USA

Dr. P. Mostafalu, Prof. S. Sonkusale
Nanoscale Integrated Sensors and Circuits Laboratory (Nanolab)
Department of Electrical and Computer Engineering
Tufts University
Medford, MA 02155, USA

Prof. M. Akbari
Department of Mechanical Engineering
University of Victoria
Victoria, BC V8W 2Y2, Canada

Prof. N. Annabi
Department of Chemical Engineering
Northeastern University
Boston 02115-5000, USA

Prof. A. Khademhosseini
Department of Physics
King Abdulaziz University
Jeddah 21569, Saudi Arabia

drug delivery platforms has lately attracted the attention of many researchers.

A topical drug delivery patch should be able to maintain conformal contact with the skin during the body movements.[5,6] In addition, a suitable environment is needed to enable effective release of drugs in a localized and sustained manner. For example, the release of water soluble drugs and factors can be facilitated in the presence of sufficient moisture at the patch and skin interface. Moisture also enhances the healing rate of skin cuts and wounds.[7] Current strategies for topical drug delivery include releasing drugs and factors that are encapsulated within ointments, hydrogels, hydrocolloids, and polymeric dressings.[8] However, these systems are mostly passive and do not allow precise control over the release profile of drugs. With the increasing number of antibiotic resistant bacteria, development of systems that offer active control over the drug release is highly desired. Recent progress in the field of polymer science has enabled scientists to synthesize and identify materials that are responsive to different stimuli including thermal, electrical, and magnetic pulses as an alternative approach to tune the drug release profile by stimulating the drug carriers in a controllable fashion. Thermal stimulation has been proven to be harmless for topical applications and thus locally heating drug carriers might be an effective approach for on demand release of drugs and factors.[9] Among thermoresponsive materials, N-Isopropylacrylamide (NIPAM) has attracted the attention of several researchers for developing drug carriers. NIPAM is a thermoresponsive material that is hydrophilic at low temperatures and becomes hydrophobic at temperatures above its critical point (≈32 °C), which can be increased by co-polymerizing it with other monomers.[10] Poly (NIPAM) hydrogels show similar behavior and possess high water content at low temperatures while the polymeric networks shrink above a critical temperature to release the water content from the gels. The critical temperature of NIPAM can be tuned and increased to even above 37 °C through copolymerization with other groups. Thus, for epidermal applications where the skin surface temperature is less than 37 °C (an average of 31–32 °C),[11] a small generated heat is sufficient to initiate the drug release through water diffusion from the hydrogel network.

Recent advances in the field of flexible and wearable electronics have enabled scientists to create devices that can form conformal contact with the skin.[12] These flexible systems can be engineered by the utilization of free-standing metallic patterns or by the fabrication of electric circuits on a flexible substrate using screen-printing.[13] The latter approach enables the integration of drug-loaded substrates with the flexible electrical system.

Here, we engineer a hydrogel-based dermal patch with integrated flexible heating elements for on-demand delivery of drugs and growth factors. The proposed patch is composed of thermoresponsive drug microcarriers that are loaded in a Ca-alginate hydrogel sheet and micropatterned gold heating elements. Monodisperse thermoresponsive particles are fabricated from NIPAM using microfluidic emulsion technique. Precise control of the patch temperature is achieved by a heating element that is connected to a microcontroller. This system can apply electrical current to the flexible heater, in order to control and stabilize the patch temperature. Integration of the electronic components into the system is achieved in a compact package to create a flexible and wearable platform (schematic shown in **Figure 1**a). The physical properties of the fabricated particles are characterized and their release profiles are determined using two different active molecules with different molecular weights resembling drugs and growth factors.

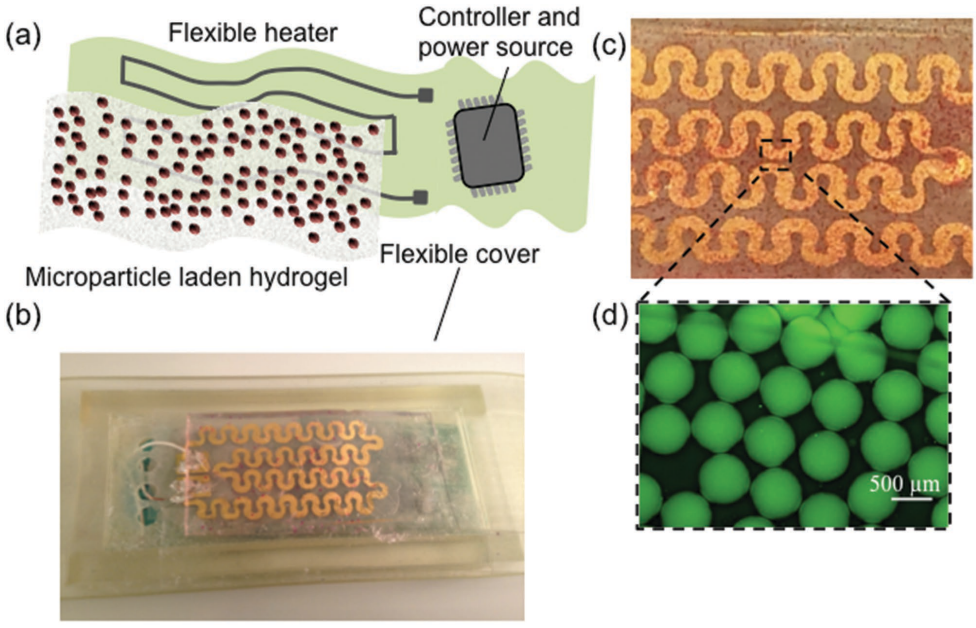

Figure 1. Fabricated wound dressing integrated with microcarriers loaded with drugs and electronics. a) Schematic showing different elements of the wound dressing. b) A representative image of the integrated wound dressing. c) Close-up view of the fabricated heater on a flexible substrate. d) The self-standing microparticles loaded with FITC-dextran.

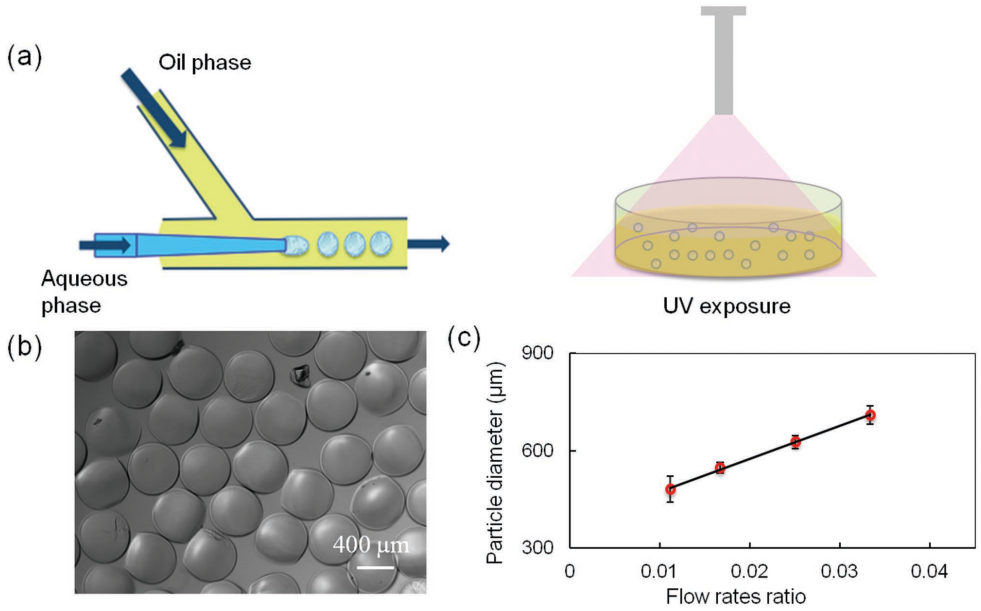

Figure 2. Fabrication and characterizations of thermoresponsive microparticles. a) Schematic illustration of flow focusing microfluidic device for microparticle fabrication. b) Microscopic image of the collected particles. c) Size of the microparticles versus the ratio of oil phase to aqueous phase flow rates.

2. Results and Discussion

The restoration of normal functionality of the skin including its regeneration ability in some cases requires intervention. For example, in the case of burns and large cuts where the microvessels are damaged, the regeneration rate of blood vessels is not sufficient to provide nutrients and factors that are required for the repair of the epidermis layer. It has been shown that in these cases providing growth factors such as vascular endothelial growth factor (VEGF) and keratinocyte growth factor (KGF) promotes the regeneration process.[14] Other factors, required to create a supportive environment for the healing process include sufficient moisture and oxygen supply and protection against pathogens. Here, we engineered a multicomponent platform that allows creating a suitable growth and regeneration environment for the skin while enabling controlled release of growth factors and antibacterial drugs.

Since the body temperature is almost constant, the use of thermoresponsive drug carriers with critical temperature slightly higher than that of the surrounding tissue might be an interesting approach for controlled drug release. PNIPAM was used herein as an example to develop a thermoresponsive platform. The key components of the platform, shown in Figure 1, include thermoresponsive microparticles, a flexible hydrogel layer, a heater for stimulating the microparticles, a controller, and a power source to adjust the generated heat, and a flexible cover that holds the components in place.

Generating a reproducible and programmable release profile can be achieved by utilization of monodisperse drug carriers.[15,16] Among different fabrication techniques for hydrogel drug carriers, emulsion method (droplet-based fluidic) is capable of high throughput fabrication of monodisperse microcarriers in the range of few micrometers to several millimeters.[16,17] Thus, we fabricated a flow-focusing device where an inner tubing with the diameter of 360 µm was placed concentric into a circular channel of 820 µm in diameter (**Figure 2**a). A solution of NIPAM (4%–10% w/v), N,N-methylene-bis-acrylamide (BIS, 0.3% w/v) as the crosslinking agent, and water soluble photoinitiator (PI, 0.5% w/v) was injected through the inner tube, while a solution of mineral oil containing 20% v/v Span80 was flowed through the sideline to surround the inner tube. As shown in Figure 2b, the fabricated particles were monodisperse. The ratio between the flow rates (Q) was adjusted to control the particle diameter and monodispersity of the particles. Figure 2c shows that for a 10% w/v solution of NIPAM the particle sizes were changed from ≈440 to 720 µm for the core (aqueous phase) to the sheath (oil phase) ratio of 0.01 and 0.033, respectively. To form crosslinked poly(NIPAM) particles, the droplets were exposed to UV light (4.3 W cm^{-2}) for 5 min keeping at a temperature around 4 °C. The particles were then washed to remove oil residues. The chemical mechanism of crosslinking is shown in Figure S1 (Supporting Information).

The turbidity and the size of the PNIPAM particles changed when they were heated above the critical temperature (≈32 °C) due to transition from hydrophilic state to hydrophobic state (**Figure 3**a). A typical time-lapse micrograph of the microparticles fabricated with 10% w/v NIPAM solution is shown in Figure 3a representing the effect of temperature variation on particles' size and turbidity. In Figure 3b, the effect of the ratio between flow rates of the core (PNIPAM 10% w/v) and sheath stream (Q) on the diameter of particles is illustrated as a function of temperature. The results suggest a relatively sharp variation in the diameter of the particles as the temperature was increased. Regardless of the initial diameter, the shrinkage starts at 32 °C. The dimensionless values for the percentage of particle diameter reduction ($100 \times (\Delta d/d_0)$) were almost constant for the tested diameters showing no statistically

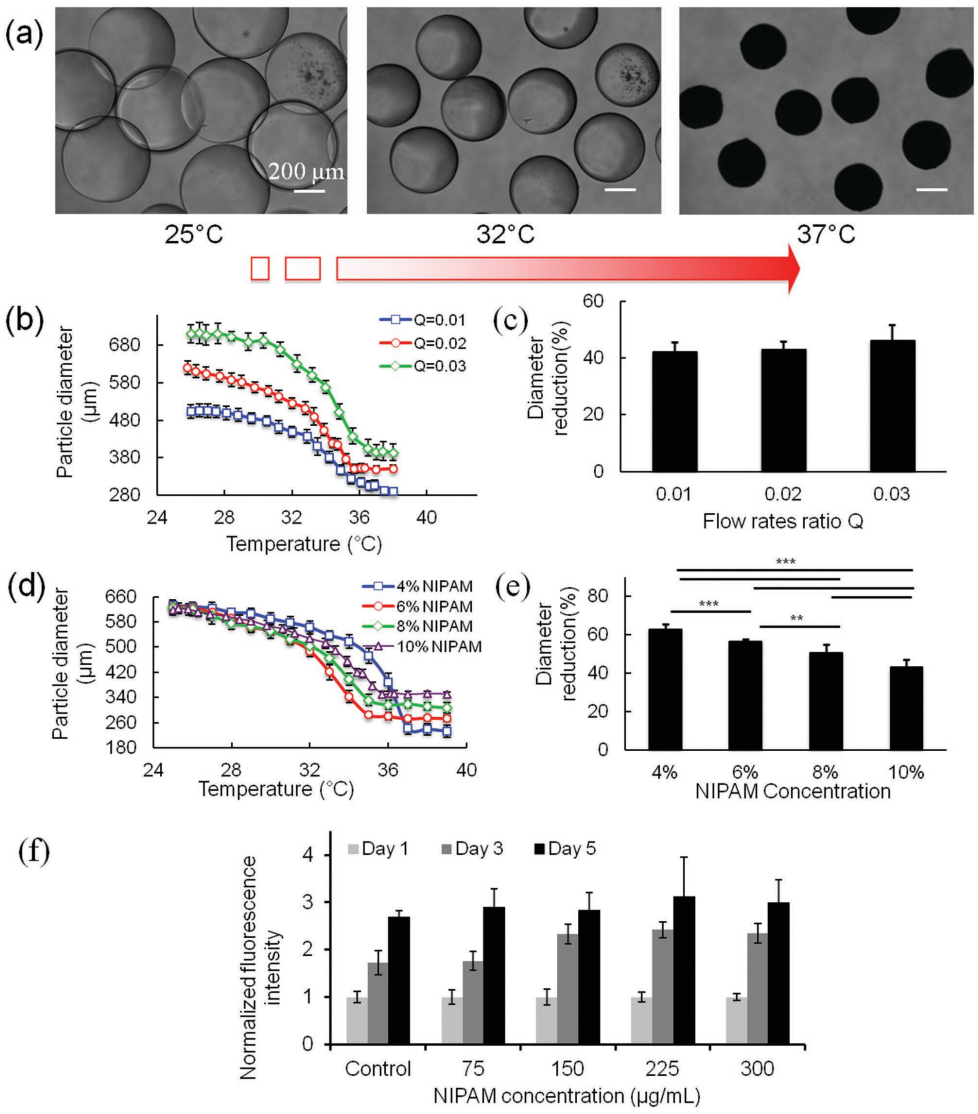

Figure 3. Physical and biological characterization of PNIPAM microparticles. a) Snapshots of shrinking of the thermoresponsive PNIPAM (10% w/v) microparticles at different temperatures. b) Variations in the microparticles' diameter with different initial size as the temperature was varied from 25 °C to 40 °C (10% NIPAM). c) Diameter shrinkage ratio for microparticles obtained using different microfluidic flow rate ratios (10% NIPAM). d) Variation of the microparticles' diameter with different NIPAM concentrations as the temperature was varied from 25 to 40 °C. e) Diameter shrinkage ratio for microparticles obtained using different NIPAM concentrations. f) The metabolic activity of keratinocytes cultured with different NIPAM concentrations in the media; cell viability was measured using Presto Blue fluorometric indicator (*$p < 0.05$, **$p < 0.01$, and ***$p < 0.001$).

significant difference between the groups (Figure 3c). The effect of NIPAM concentration on the particles' response was studied; as shown in Figure 3d,e, the variation in particle diameter was more pronounced in microparticles fabricated with lower NIPAM concentrations.

Since the transparency of PNIPAM microparticles changed with temperature, UV–vis absorption spectrometry was used to investigate their temperature sensitivity.[18] The results indicated that changing the PI concentration did not interfere with the critical temperature at which the polymer's turbidity abruptly shifted upon heating which, was around 32 °C (Figure S2, Supporting Information) and all samples reached a plateau around 37 °C; however the extent of the turbidity alteration between 29 and 43 °C increased by decreasing PI concentration. The dynamic response of the microparticles with different polymer concentrations to temperature variation was also monitored over the temperature ranging from 29 to 43 °C (Figure S3, Supporting Information). Higher NIPAM concentrations resulted in slightly delayed critical temperature upon heating; the expansion of all the samples during their cool down process was found to be slower.

Another important factor prior to utilization of PNIPAM microparticles in topical drug delivery is to confirm their biocompatibility. Thus, we cultured human keratinocytes and exposed them to different concentrations of PNIPAM particles. We incubated the samples with cells and then assessed the cellular metabolic activity by Presto Blue assay. The results in Figure 3f demonstrate that there was not a significant difference between the metabolic activities of treated and control cells, which confirms the cytocompatibility of the fabricated PNIPAM microparticles for topical applications.

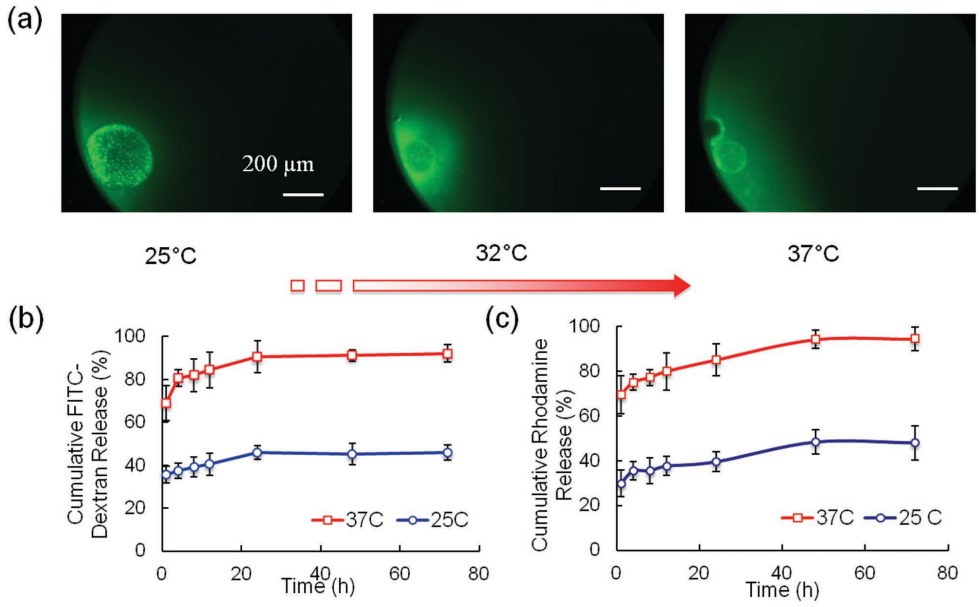

Figure 4. Drug release from the thermoresponsive particles. a) Snapshot of release of FITC-dextran from particles incubated in PBS during heating. b) Cumulative release of FITC-dextran (M_w 70 000) from PNIPAM particles at different temperatures. c) Cumulative release of rhodamine isocyanate (M_w 536.08) from PNIPAM particles at different temperatures.

We also examined the swelling characteristics of different concentrations of PNIPAM in a test solution with ionic composition comparable to human serum following standardized assay (BS EN 13726-1) at 25 and 37 °C over the course of 48 h (Figure S4, Supporting Information). The results indicated a strong effect of temperature on the absorbance capacity of PNIPAM, showing initial shrinking at 25 °C and swelling at 37 °C before reaching a plateau. Higher concentrations of NIPAM turned out to be more resistant to absorbance at both temperatures.

There are various parameters that can affect the release kinetics and drug delivery properties.[19] Here, we studied the release profile of two drug models with different molecular weights keeping the particle size, concentrations, crosslinking process, and drug loading method constant. Fluorescein isothiocyanate-dextran (FITC-dextran) with molecular weight of 70 kDa was used that has a molecular weight comparable to many growth factors such as VEGF and KGF. In addition, we used rhodamine isocyanate with the molecular weight of 536.08 Da that is in the size range of some commercial antibiotics used for treating skin infections. Both active molecules are fluorescent and can be easily detected using a spectrophotometer. In **Figure 4**a, a set of time-lapse micrographs shows the release of FITC-dextran from a microparticle into the surrounding Phosphate-buffered saline (PBS) upon heating. For this purpose, a single FITC-dextran loaded microparticle was placed in a cavity on a transparent holder filled with 100 µL of PBS. The holder was then mounted on a glass slide and placed inside the environmental chamber of the microscope to observe the release of FITC-dextran in response to an increase in the temperature.

Cumulative release of FITC-dextran and rhodamine isocyanate from microparticles was measured at 25 and 37 °C over the course of 72 h (Figure 4b). The results indicated an initial burst release of both drug models. The initial burst release has been reported in many drug delivery systems. However, we expect that soaking and thorough washing of particles can reduce the amount of this burst release to some extent.[20] The initial burst release is followed by diffusive release. The observed shift in the release profiles at 25 and 37 °C may be due to initial shrinkage of the microparticles and its significant effect on the burst release at a higher temperature. At 37 °C, the particles showed a burst release of almost 70% versus about 30% at 25 °C in initial hours followed by a reduced release rate up to 72 h.

The microparticles were embedded inside a prepolymer solution which was directly casted on top of a flexible heater to minimize the interfacial thermal contact resistance. The resistance of the heater was around 80 Ω and the generated heat could be adjusted by tuning the applied current or voltage and the time duration of application (electrical power = I^2R or V^2/R, where R is the resistance of the heater, I is the electrical current, and V is voltage). To activate the flexible heater and achieve a stable temperature, a set of off-the-shelf electronic components were utilized. Current drive circuitry was used to power up the heater (**Figure 5**a). A LightBlue Bean microcontroller board (Figure 5b) was also employed to control the driver board by programming the applied electrical current to the heater and consequently adjusting the hydrogel temperature. To control the temperature of thermoresponsive particles in the hydrogel sheet, a flexible heater was designed and microfabricated as described in details in the Experimental Section (Figure 5c,d). As shown in Figure 5e, the temperature reached 35 °C starting from 23 °C in less than 1 min and then it remained stable during the delivery process. This system can be later integrated with a temperature sensor to enable a more precise temperature adjustment.

To create an environment that supports the release of water soluble factors while maintaining the moisture level

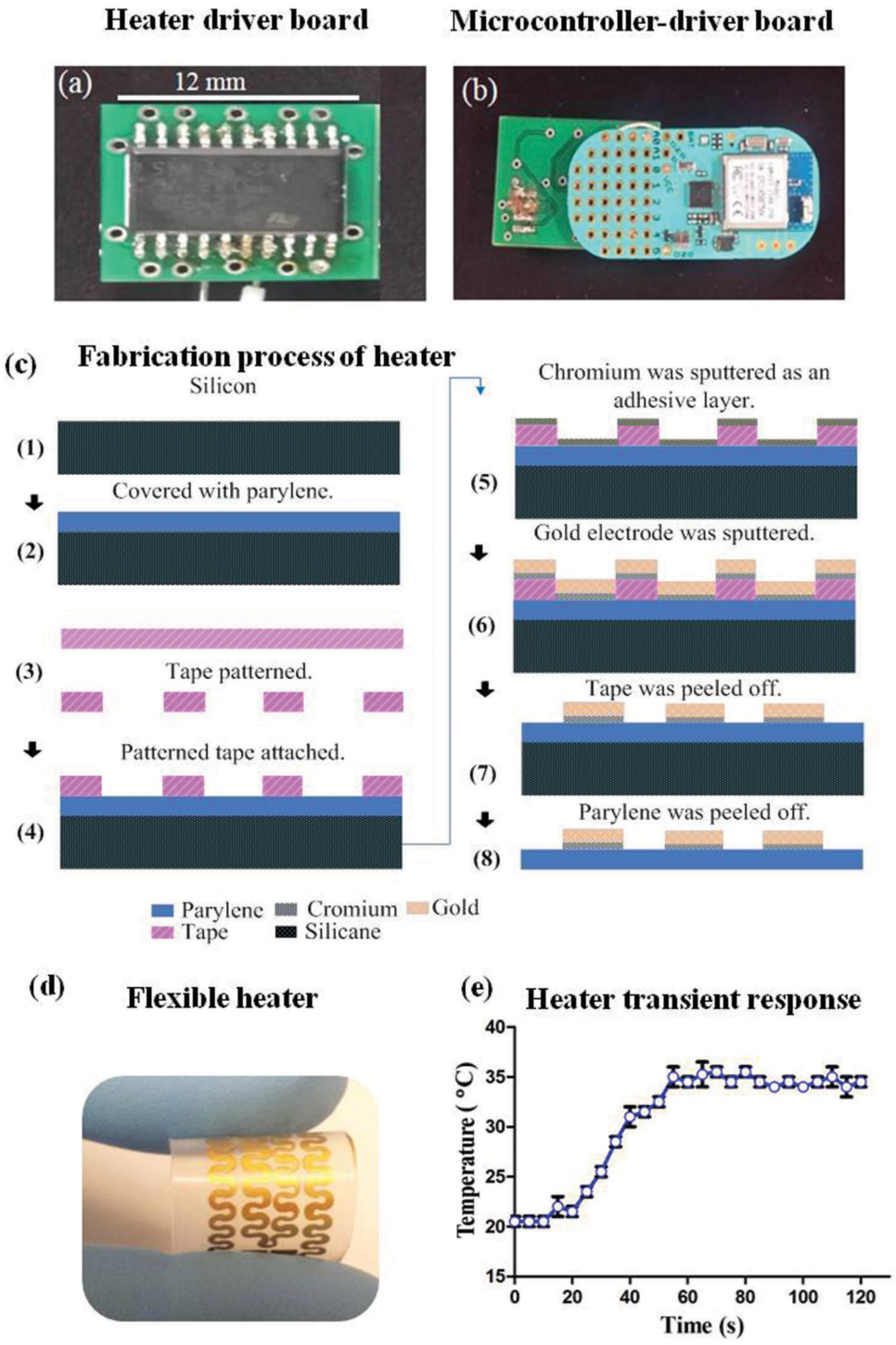

Figure 5. The electronic components and the fabrication method for the flexible patch system. a) Photograph of the heater circuitry. b) Photograph of the integrated microcontroller (LightBlue Bean) and electronics. c) Fabrication process of the flexible heater on parylene. d) Optical image of the microfabricated flexible heater. e) Transient response of the heater over 2 min.

in the wound area, we employed a hydrogel sheet to create a wet dermal patch. Thus, drug loaded microparticles were embedded in an alginate-based hydrogel patch. **Figure 6**a describes the steps carried out for crosslinking of the microparticle laden hydrogel patch in a flat Polydimethylsiloxane (PDMS) mold. To ensure the flatness of the hydrogel sheet, the mixture of sodium alginate (Na-alginate) and microparticles were covered with a flat sheet of agarose gel containing $CaCl_2$ aqueous solution. The Na-alginate was crosslinked by exchanging Na^+ with Ca^{2+} to form a hydrogel network of

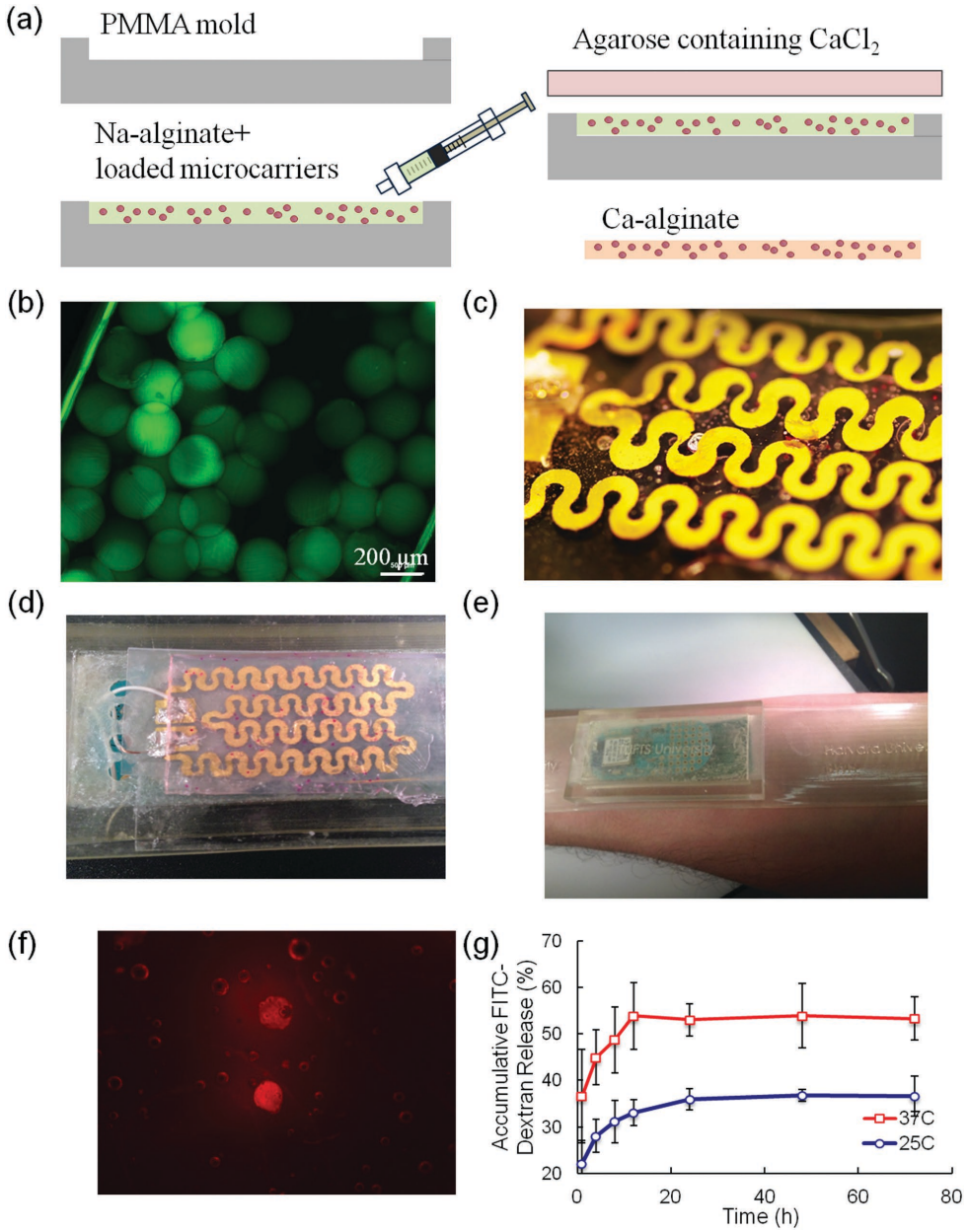

Figure 6. The integrated platform for epidermal drug delivery. a) Schematic illustration of the fabrication steps for the hydrogel patch. b) Top view of the alginate patch with embedded PNIPAM microparticles containing FITC-dextran. c) Close-up view of the hydrogel patch with embedded microparticles, integrated with the flexible heater. d) The assembled parts including the loaded hydrogel patch, heater, temperature sensor and micro controller. e) A representative image showing the conformal contact of the engineered patch to skin. f) Fluorescence image showing rhodamine isocyanate release from particles embedded in the alginate patch after being heated by the electric heater. g) Cumulative release of FITC-dextran from particles embedded in the alginate patch.

calcium alginate. Figure 6b represents the fluorescent micrograph of a typical alginate sheet with embedded monodisperse PNIPAM microparticles that were loaded with FITC-dextran. The process enabled us to fabricate hydrogel sheets with different thicknesses. An alginate sheet with the thickness of 800 μm was found to be flexible yet strong enough to form conformal contact with skin and was used throughout the experiments. To minimize the thermal contact resistance between different layers, the flexible heater was placed at the bottom of the PDMS mold during the hydrogel fabrication process. Thus, the hydrogel sheet adhered well to the heater (Figure 6c). The drug-loaded patch, the heater, and the microcontroller were assembled on a 3D-printed TangoPlus flexible substrate (Figure 6d) to provide a conformal contact between the dermal patch and the body (Figure 6e). Incorporating different drug models in the microparticles validated the efficient release of drugs from the particles embedded in the alginate sheet. Figure 6f represents the fluorescent micrograph of rhodamine isocyanate released upon heating from particles embedded in the alginate sheet, where an increase in the fluorescent intensity could be

observed in the parts of the hydrogel surrounding the particles. Percent cumulative release of FITC-dextran from particle-laden alginate patch was measured by placing it into a PBS solution at constant temperatures of 25 and 37 °C over the course of 72 h (Figure 6g). The key advantage of the proposed system is the faster and on demand release of molecules compared to passive diffusion. The critical temperature of NIPAM, as an example for thermoresponsive materials, is around 32 ºC, thus a sharp change was observed in the response of microparticles around 32 ºC. Since the particles are encapsulated within a thermally insulating hydrogel layer, the temperature distribution will not be uniform. Thus, by changing the applied temperature, the rate and the number of particles that can be triggered will change and thus the release rate can be relatively adjusted. The release data confirmed the substantial effect of temperature on controlling the release rate. A closer examination of the release profile revealed considerable difference in the slope of release profile, especially in the first 12 h (more than 50%) by changing the applied temperature from 25 to 37 ºC (Figure S6, Supporting Information).

The general release profile of the drugs from encapsulated microparticles is similar to that of nonencapsulated microparticles, whereas embedding the particles in the alginate sheet reduced and prolonged the release rates as expected. We also measured the release rate of FITC-dextran freely encapsulated within alginate hydrogel (Figure S5, Supporting Information). It can be seen that 24 h is required for alginate to release the encapsulated drug. This observation is in agreement with Figure 6g, where a 24 h delay was observed in FITC-dextran release in comparison to free particles (Figure 4b). Similar observations are reported for PNIPAM particles embedded in PEGDA hydrogel.[21] Overall, compared to the system of self-standing microparticles, the drug discharged from the embedded microparticles takes longer to diffuse through the hydrogel and to release in the PBS solution. In particular, the hydrogel encapsulated particles demonstrated a relatively restrained initial burst that can be attributed to the buffering effect of the hydrogel as reported in other studies where drug loaded particles were embedded inside a hydrogel matrix.[22] Apart from the drug release induced by microparticle shrinking, passive release can occur mainly by diffusion through the polymer barriers and the polymer degradation. Since the degradation times of PNIPAM (Figure S4, Supporting Information) and alginate are relatively higher than the period of the release tests,[23] diffusion can be considered as the main factor, after the accelerating effect of particle sharinkage in response to temperature rise. Based on the data in the literature reporting that hydrogel thickness can have a rate limiting effect on drug transport when diffusion is a contributing mechanism in the release,[24] we speculate that the diffusion time of the drug out of the patch can be tuned by controlling the thickness of the hydrogel layer.

The difference between release profile of self-standing microparticles and those embedded in the hydrogel can be partially attributed to limited mobility as well as the distribution of the encapsulated microparticles. Cumulative release of 92% of the drug was measured for self-standing microparticles where this amount was reduced to 53% for microparticles embedded in an alginate sheet after 72 h incubation at 37 °C. We also speculate that more sustained release profiles can be obtained by adopting approaches to reduce the number of particles located in the outer surface of the hydrogel matrix.

3. Conclusions

In this study, we engineered a topical drug delivery platform that could effectively release the required drug and growth factors for treating skin disorders such as chronic wounds and burns. This platform offers multiple attractive features including good conformability with the skin, the ability to maintain the skin moisture and protecting the wound from pathogens. In addition, it enables the possibility of controlled and on demand drug delivery. Thermoresponsive drug carriers encapsulated within hydrogel sheets offer the possibility of modulating drug release rate through controlling the applied temperature. As a proof of concept demonstration, PNIPAM monodisperse thermoresponsive drug carriers were fabricated using microfluidic emulsion process and their response to temperature variation was characterized through monitoring both particles' shrinking characteristics and UV–vis absorption spectrometry using different polymer concentrations. We demonstrated the efficient release of different drug models from self-standing particles and microparticles embedded in hydrogel sheet. In addition, the biocompatibility of the drug carriers was verified. The proposed platform was comprised of a flexible heater, temperature sensor, and microcontroller mounted on the particle laden hydrogel patch, that provide precise control on the patch temperature. Characterization of the heater response over time showed a quite short transient phase and the ability to maintain the patch temperature at the desired range over a period of time. The aforementioned components were all integrated on a flexible and wearable platform.

The drug release from the engineered patch could be tuned by controlling the composition of the particles and the thickness of the hydrogel patch. Further, the critical temperature to which microparticles respond could be adjusted based on the application by co-polymerizing NIPAM with other monomers.

In conclusion, this study paves the way to develop new solutions for accelerating the healing process of skin disorders and chronic wounds using smart drug delivery platforms. Besides the typical functions of the customary wound healing products, these platforms offer efficient control over the drug release rate and kinetics.

4. Experimental Section

Materials: Sodium alginate, calcium chloride ($CaCl_2$), NIPAM, crosslinking agent N,N′-methylenebisacrylamide, agarose, and mineral oil were purchased from Sigma Aldrich (St. Louis, MO, USA). 2-hydroxy-1-(4-(hydroxyethoxy)phenyl)-2-methyl-1-propanone (Irgacure 2959, CIBA Chemicals) was used as PI. An Omnicure S2000 UV illumination system was used for photocrosslinking of NIPAM.

Dulbecco's modified Eagle medium (DMEM), fetal bovine serum (FBS), 0.05% trypsin-Ethylenediaminetetraacetic acid (EDTA) (1X), and antibiotics (penicillin/streptomycin) were purchased from Invitrogen (Carlsbad, CA, USA). PrestoBlue cell viability reagent was obtained from Life Technologies.

Microparticles Fabrication and Microfluidic Device Characterization: Monodisperse and thermally responsive microparticles were fabricated using a microfluidic flow-focusing device. A cylindrical capillary tube was

coaxially aligned within a channel fabricated in the PDMS device. The inner diameters of the injection tube and PDMS channel were 360 and 820 μm, respectively. NIPAM was purified by recrystallization with a hexane/acetone mixture (50/50 v/v). The dispersed inner phase was an aqueous solution of NIPAM (4%–10% w/v), N,N-methylene-bis-acrylamide (BIS, 0.3% w/v) as the crosslinking agent, and water soluble PI (0.5% w/v). The continuous phase was mineral oil containing 20% v/v of nonionic surfactant Span80. The two phases were injected into the inlets of the microfluidic device using plastic syringes (BD Biosciences) connected by chemical resistant clear PVC tubing (Mcmaster-carr). The flow rates of the solutions were finely controlled by syringe pumps (PHD 2000, Harvard Apparatus).

The microparticles were collected in a Petri dish and then were photopolymerized through exposure to UV light for 5 min, keeping the temperature around 4 °C to reduce the reaction rate. The UV intensity was set to 850 mW and the distance between the tip of the fiber optic cable and the Petri dish was set to 8 cm. The crosslinked microparticles were then washed in DI water and the surfactant four times by centrifugation in order to remove the excess oil. The formation of the particles and the effect of flow rate variation on particle size were monitored using an inverted optical microscope (TE2000-U, Nikon).

Characterization of the Thermoresponsive Behavior of the Microparticles: The thermoresponse of the fabricated microparticles was characterized by raising their ambient temperature from 25 to 40 °C. The PNIPAM microparticles at room temperature were put in multiwell plates and were then placed on a Zeiss Axio observer D1 microscope equipped with an environmental chamber and a heating unit (XL S Zeiss). The temperature was slowly increased (1 °C min^{-1}) and the microparticles' ambient was measured continuously by the thermometer placed in the chamber. For each case 40 particles were monitored and the images were later analyzed using ImageJ[25] to characterize their thermoresponsive behavior.

As the temperature was increased, the PNIPAM particles shrink and become opaque. In order to investigate the response of the crosslinked PNIPAM, the variations of UV–vis absorption of the crosslinked microparticles as a function of monomer concentration (4–10 w/v%) and PI concentration (0.5–0.125 w/v%) were determined a BioTek UV/vis Synnergy 2 spectrophotometer over a range of temperatures (28–42 °C).

Hydrogel Patch Preparation: The thermoresponsive microparticles were encapsulated within an alginate-based hydrogel patch. A solution of sodium alginate (Na-alginate; 2% w/v) was dissolved in distilled water and stored at 4 °C. Microparticles were mixed with the Na-alginate solution prior to use. To crosslink and form an alginate sheet, an aqueous solution of calcium chloride ($CaCl_2$; 2% w/v) and agarose (2% w/v) was poured in to a PDMS flat mold and left at room temperature for 30 min to solidify. The agarose sheet was then peeled off and stored. The alginate solution was poured into another PDMS mold and the sheet obtained from the solidified $CaCl_2$ and agarose sheet was used to cover the Na-alginate for few minutes until calcium alginate sheets were formed.

Release Studies: Freeze dried microparticles were weighed and soaked in either a fluorescein isothiocyanate-dextran (FITC-dextran, M_w 70 kDa) solution (1 mg mL^{-1}) or rhodamine isocyanate (M_w 536.08 Da) solution (1 mg mL^{-1}) and incubated for 24 h to swell and absorb the drug solution. Both reagents are fluorescent and can be detected using a UV–vis spectrophotometer. For both batches, the microparticles were then separated from the solution and washed in order to remove the excess drug solution from their surfaces. Similar weights (2 mg) of loaded particles were then separately added to 2 mL PBS and multiple containers were kept at different temperatures. At each time point, 200 μL of the supernatant was removed and used to measure its fluorescent intensity (FITC-dextran: λ_{ex} 485 nm and λ_{em} 530 nm; rhodamine isocyanate: λ_{ex} 543 nm and λ_{em} 580 nm). A calibration curve was prepared by measuring the intensities of known concentrations and was used to determine the concentration of the released drug models (FITC-dextran and rhodamine isocyanate). The results were then normalized and converted to percentage cumulative release. In all our release experiments, a similar drug delivery system without the loaded drug was used as the background signal.

Cell Studies: Human keratinocytes were cultured in a DMEM supplemented with 10% FBS and 1% penicillin/streptomycin at 37 °C and 5% CO_2. Cells were passaged at ≈80% confluency.

For cytotoxicity assessment, cells were trypsinized and then seeded in 48-well polystyrene plates at the concentration of 5×10^3 cells per well. Cells were then treated with different quantities of PNIPAM particles and their metabolic activity was monitored using PrestoBlue assay. The blue stain PrestoBlue reagent was uptaken by viable cells and reduced to a fluorescing stain. The extent of reduction is directly proportional to the cells' proliferation. The assay was performed on days 1, 3, and 5 as per manufacturer's recommended protocol and the reduction induced colour change was measured using a BioTek UV/vis Synnergy 2 microplate reader.

Free Swell Absorbance Capacity Tests: Swelling tests were performed following the procedure suggested in BS EN 13726-1: Test Methods for Primary Wound Dressings – Aspects of Absorbency. This approach assesses the performance of the different concentrations of PNIPAM when it is typically exposed to moderately to heavily exudating wounds. PDMS molds were used to prepare samples of the same shape and size for different hydrogels. Crosslinked hydrogel samples were soaked in test solution that was an aqueous solution of Na^+ (142 mmol) and Ca^{2+} (2.5 mmol) with an ionic composition comparable to human serum and wound exudate, as suggested by the BS EN 13726-1 standard. At each time point the samples were taken out of the solution, the excess solution on their surface was removed and the samples were weighed using a high precision scale. The free swell absorbance tests were carried out both at 25 and 37 °C.

Electronics Assembly into the Patch and Characterization: A localized bandage platform was fabricated from a microfabricated flexible heater, microparticle loaded hydrogel, a compact assembly of off-the-shelf electronic components covered by a flexible plastic casing. The miniaturized system was wearable and flexible and could activate the heater and stabilize the temperature in the range of 32–37 °C.

The heater with resistance of ≈80 Ω was microfabricated on a parylene-C substrate. First, a silicon wafer was covered by 12 μm of parylene-C, using a PDS2010 parylene coater with 20 g of dimer at room temperature. An adhesive stencil tape was patterned by a laser cutter (Versa, VLS2.40) (power 40%, speed 20%) and was attached to the parylene substrate. Then, 15 nm chromium and 150 nm gold was sputtered on the substrate. The stencil was then peeled off, leaving behind the flexible microfabricated heater.

A microcontroller (Arduino) was used to control the current driver (L293) and amount of the power transferred to the heater. Moreover, feedback from noncontact infrared thermometer (Cason, USA) was used to stabilize and calibrate the hydrogel temperature. Response time of the heater was measured to be 2 min. The flexible heater and microcontroller were integrated on a 3D-printed flexible casing using TangoPlus (FLX930) that is an extremely flexible elastomer with 218% elongation at the break point and Young's modulus of 1.5 MPa, which is comparable to human epidermis.[5]

Supporting Information

Supporting Information is available from the Wiley Online Library or from the author.

Acknowledgements

S.B. and A.T. contributed equally to this work. S.B. acknowledges funding from MIT-Italy program (Progetto Rocca) and Polimi International Fellowship (PIF). A.K., P.M., S.S., M.R.D., and A.T. acknowledge funding from the National Science Foundation (EFRI-1240443), the office of Naval Research Young National Investigator Award, and the National Institutes of Health (HL092836, DE019024, EB012597, AR057837, DE021468, HL099073, EB008392).

[1] Y. Bayram, M. Parlak, C. Aypak, I. Bayram, *Int. J. Med. Sci.* **2013**, *10*, 19.

[2] a) M. M. Martino, F. Tortelli, M. Mochizuki, S. Traub, D. Ben-David, G. A. Kuhn, R. Müller, E. Livne, S. A. Eming, J. A. Hubbell, *Sci. Trans. Med.* **2011**, *3*, 100ra89; b) B. Behm, P. Babilas, M. Landthaler, S. Schreml, *J. Eur. Acad. Dermatol. Venereol.* **2012**, *26*, 812.

[3] a) R. D. Galiano, O. M. Tepper, C. R. Pelo, K. A. Bhatt, M. Callaghan, N. Bastidas, S. Bunting, H. G. Steinmetz, G. C. Gurtner, *Am. J. Pathol.* **2004**, *164*, 1935; b) I. R. Edwards, J. K. Aronson, *The Lancet* **2000**, *356*, 1255.

[4] a) M. R. Prausnitz, S. Mitragotri, R. Langer, *Nat. Rev. Drug Discov.* **2004**, *3*, 115; b) M. R. Prausnitz, R. Langer, *Nat. Biotechnol.* **2008**, *26*, 1261.

[5] J. L. Gennisson, T. Baldeweck, M. Tanter, S. Catheline, M. Fink, L. Sandrin, C. Cornillon, B. Querleux, *IEEE Trans. Ultrason., Ferroelectrics Freq. Control.* **2004**, *51*, 980.

[6] M. Geerligs, Thesis, *Tech. Univ. Eindhoven* **2010**.

[7] S. Guo, L. A. DiPietro, *J. Dental Res.* **2010**, *89*, 219.

[8] a) B. W. Barry, *Eur. J. Pharm. Sci.* **2001**, *14*, 101; b) J. Hadgraft, *Int. J. Pharm.* **1999**, *184*, 1; c) A. Naik, Y. N. Kalia, R. H. Guy, *Pharm. Sci. Technol. Today* **2000**, *3*, 318.

[9] a) N. Annabi, A. Tamayol, J. A. Uquillas, M. Akbari, L. E. Bertassoni, C. Cha, G. Camci-Unal, M. R. Dokmeci, N. A. Peppas, A. Khademhosseini, *Adv. Mater.* **2014**, *26*, 85; b) D. Schmaljohann, *Adv. Drug Deliv. Rev.* **2006**, *58*, 1655.

[10] H. Wei, S.-X. Cheng, X.-Z. Zhang, R.-X. Zhuo, *Prog. Polym. Sci.* **2009**, *34*, 893.

[11] B. W. Olesen, *Tech. Rev.* **1982**, *2*, 3.

[12] a) D.-H. Kim, N. Lu, R. Ma, Y.-S. Kim, R.-H. Kim, S. Wang, J. Wu, S. M. Won, H. Tao, A. Islam, *Science* **2011**, *333*, 838; b) A. H. Najafabadi, A. Tamayol, N. Annabi, M. Ochoa, P. Mostafalu, M. Akbari, M. Nikkhah, R. Rahimi, M. R. Dokmeci, S. Sonkusale, *Adv. Mater.* **2014**, *26*, 5823; c) P. Mostafalu, W. Lenk, M. Dokmeci, B. Ziaie, A. Khademhosseini, S. Sonkusale, *in IEEE Biomedical Circuits and Systems Conf. (BioCAS), IEEE, Lausanne, Switzerland* **2014**.

[13] a) K. Fujimoto, G. Bonmassar, A. J. Golby, *PLoS One* **2012**, *7*, e41187; b) D.-H. Kim, N. Lu, R. Ma, Y.-S. Kim, R.-H. Kim, S. Wang, J. Wu, S. M. Won, H. Tao, A. Islam, K. J. Yu, T.-I. Kim, R. Chowdhury, M. Ying, L. Xu, M. Li, H.-J. Chung, H. Keum, M. McCormick, P. Liu, Y.-W. Zhang, F. G. Omenetto, Y. Huang, T. Coleman, J. A. Rogers, *Science* **2011**, *333*, 838; c) D.-H. Kim, J. Viventi, J. J. Amsden, J. Xiao, L. Vigeland, Y.-S. Kim, J. A. Blanco, B. Panilaitis, E. S. Frechette, D. Contreras, D. L. Kaplan, F. G. Omenetto, Y. Huang, K.-C. Hwang, M. R. Zakin, B. Litt, J. A. Rogers, *Nat. Mater.* **2010**, *9*, 511; d) P. Mostafalu, S. Sonkusale, *RSC Adv.* **2015**, *5*, 8680.

[14] a) G. Marti, M. Ferguson, J. Wang, C. Byrnes, R. Dieb, R. Qaiser, P. Bonde, M. Duncan, J. Harmon, *Gene Therapy* **2004**, *11*, 1780; b) N. N. Nissen, P. Polverini, A. E. Koch, M. V. Volin, R. L. Gamelli, L. A. DiPietro, *Am. J. Pathol.* **1998**, *152*, 1445.

[15] a) A. Abbaspourrad, S. S. Datta, D. A. Weitz, *Langmuir* **2013**, *29*, 12697; b) W. J. Duncanson, T. Lin, A. R. Abate, S. Seiffert, R. K. Shah, D. A. Weitz, *Lab Chip* **2012**, *12*, 2135.

[16] S. S. Datta, A. Abbaspourrad, E. Amstad, J. Fan, S.-H. Kim, M. Romanowsky, H. C. Shum, B. Sun, A. S. Utada, M. Windbergs, S. Zhou, D. A. Weitz, *Adv. Mater.* **2014**, *26*, 2205.

[17] R. Riahi, A. Tamayol, S. A. M. Shaegh, A. M. Ghaemmaghami, M. R. Dokmeci, A. Khademshosseini, *Curr. Opin. Chem. Eng.* **2015**, *7*, 101.

[18] T. Wu, Z. Ge, S. Liu, *Chem. Mater.* **2011**, *23*, 2370.

[19] C.-C. Lin, A. T. Metters, *Adv. Drug Deliv. Rev.* **2006**, *58*, 1379.

[20] R. Lin, L. Shi Ng, C.-H. Wang, *Biomaterials* **2005**, *26*, 4476.

[21] R. M. K. Ramanan, P. Chellamuthu, L. Tang, K. T. Nguyen, *Biotechnol. Prog.* **2006**, *22*, 118.

[22] a) D.-H. Kim, D. C. Martin, *Biomaterials* **2006**, *27*, 3031; b) J. Liu, S. M. Zhang, P. P. Chen, L. Cheng, W. Zhou, W. X. Tang, Z. W. Chen, C. M. Ke, *J. Mater. Sci.: Mater. Med.* **2007**, *18*, 2205.

[23] a) J. Qian, F. Wu, *J. Mater. Chem. B* **2013**, *1*, 3464; b) M. Akbari, A. Tamayol, V. Laforte, N. Annabi, A. H. Najafabadi, A. Khademhosseini, D. Juncker, *Adv. Funct. Mater.* **2014**, *24*, 4060.

[24] a) J. Kim, A. Conway, A. Chauhan, *Biomaterials* **2008**, *29*, 2259; b) J.-C. Gayet, G. Fortier, *J. Controll. Rel.* **1996**, *38*, 177.

[25] C. A. Schneider, W. S. Rasband, K. W. Eliceiri, *Nat. Methods* **2012**, *9*, 671.